Micelle-Induced Folding of Spinach Thylakoid Soluble Phosphoprotein of 9 kDa and Its Functional Implications[†,‡]

Jikui Song,[§] Min S. Lee,[§] Inger Carlberg,[||] Alexander V. Vener,[⊥] and John L. Markley*[,§]

Center for Eukaryotic Structural Genomics, Department of Biochemistry, University of Wisconsin−Madison, Wisconsin 53706-1544, Department of Biochemistry and Biophysics, Arrhenius Laboratories of Natural Sciences, Stockholm University, SE-10691 Stockholm, Sweden, and Division of Cell Biology, Linköping University, SE-58185 Linköping, Sweden

Received October 16, 2006; Revised Manuscript Received October 20, 2006

ABSTRACT: Thylakoid soluble phosphoprotein of 9 kDa (TSP9) has been identified as a plant-specific protein in the photosynthetic thylakoid membrane (Carlberg et al. (2003) *Proc. Natl. Acad. Sci. 100*, 757−762). Nonphosphorylated TSP9 is associated with the membrane, whereas, after light-induced phosphorylation, a fraction of the phosphorylated TSP9 is released into the aqueous stroma. By NMR spectroscopy, we have determined the structural features of nonphosphorylated TSP9 both in aqueous solution and in membrane mimetic micelles. The results show that both wild type nonphosphorylated TSP9 and a triple-mutant (T46E + T53E + T60E) mimic of the triphosphorylated form of TSP9 are disordered under aqueous conditions, but adopt an ordered conformation in the presence of detergent micelles. The micelle-induced structural features, which are similar in micelles either of SDS or dodecylphosphocholine (DPC), consist of an N-terminal α-helix, which may represent the primary site of interaction between TSP9 and binding partners, and a less structured helical turn near the C-terminus. These structured elements contain mainly hydrophobic residues. NMR relaxation data for nonphosphorylated TSP9 in SDS micelles indicated that the molecule is highly flexible with the highest order in the N-terminal α-helix. Intermolecular NOE signals, as well as spin probe-induced broadening of NMR signals, demonstrated that the SDS micelles contact both the structured and a portion of the unstructured regions of TSP9, in particular, those containing the three phosphorylation sites (T46, T53, and T60). This interaction may explain the selective dissociation of phosphorylated TSP9 from the membrane. Our study presents a structural model for the role played by the structured and unstructured regions of TSP9 in its membrane association and biological function.

The central player in plant photosynthesis is photosystem II (PSII[1]) in the thylakoid membrane (*1*, *2*), which absorbs solar energy and catalyzes the splitting of water into dioxgen and reducing equivalents. The light-harvesting complex II (LHCII), peripheral to the PSII, helps to increase the effective energy absorption by PSII (*3*). The photosynthetic process in this PSII−LHCII multisubunit complex is regulated by a unique light- and redox-controlled protein phosphorylation system (*4*, *5*). In response to light, the plastoquinol pool becomes reduced (*6*, *7*), leading to the activation of protein kinases in the thylakoid membrane (*8*−*11*). These activated protein kinases subsequently phosphorylate PSII, LHCII, and other polypeptide substrates (*5*, *12*−*15*). Phosphorylation of PSII and LHCII further causes the redistribution of absorbed light energy by state transition of LHCII (*4*, *16*−*20*): migration of LHCII from the PSII to the PSI, which decreases absorption of light by PSII and increases absorption of light by PSI. The cascade of phosphorylation is eventually reversed by a phosphatase (*21*, *22*), and the dephosphorylated LHCII returns to PSII. Thus far, a number of phosphoproteins in the PSII−LHCII supercomplex have been identified (*15*, *20*, *21*, *23*−*26*). Characterization of the structural and functional consequences of the phosphorylation of these proteins is of obvious interest in further understanding the process of the state transitions and regulation of photosynthetic light harvesting.

The thylakoid soluble phosphoprotein of 9 kDa (here we use the abbreviation TSP9 to refer to the nonphosphorylated form of this protein) is one of the recently characterized phosphoproteins in the thylakoid membrane (*21*, *27*). In contrast to the other identified thylakoid phosphoproteins that

[†] This work was supported by NIH Grants P50 GM64598 and U54 GM074901 from the National Institute of General Medical Sciences (J.L.M., P.I). NMR data were collected at the National Magnetic Resonance Facility at Madison, which is supported in part by NIH Grants P41 RR02301 and P41 GM66326.

[‡] Structure determined under the National Institutes of Health, NIGMS Protein Structure Initiative; coordinates and related data have been deposited at the PDB (2FFT) and NMR data at BMRB (bmr 6926).

* To whom correspondence should be addressed. Department of Biochemistry, University of Wisconsin−Madison, Madison, WI 53706. Tel: (608) 263-9349. Fax: (608) 262-3759. E-mail: markley@nmrfam.wisc.edu.

[§] University of Wisconsin−Madison.

[||] Stockholm University.

[⊥] Linköping University.

[1] Abbreviations: COSY, correlated spectroscopy; DPC, dodecylphosphocholine; HSQC, heteronuclear single-quantum correlation; LHCII light-harvesting complex II; NOE, nuclear Overhauser effect; NOESY, NOE spectroscopy; PSII, photosystem II; SDS, sodium dodecyl sulfate; TALOS, torsion angle likelihood obtained from shift and sequence similarity; TEV, tobacco etch virus; TSP9, nonphosphorylated form of thylakoid soluble phosphoprotein of 9 kDa; TSP9-(T46E+T53E+T60E), triple-mutant of TSP9 with residue substitutions at the three phosphorylation sites that mimic phosphorylation; 5-DSA, 5-doxylstearic acid; 16-DSA, 16-doxylstearic acid.

10.1021/bi062148m CCC: $33.50
Published on Web 12/08/2006

are integrated into the membrane, TSP9 is a peripheral protein found partly in the soluble stroma fraction (*27*). Cross-linking experiments have localized spinach TSP9 with LHCII and at the interface between LHCII and PSII (*28*). Although the molecular function of TSP9 remains unclear, it has been observed that the phosphorylation of TSP9 and its sensitivity to inhibitors were very similar to those for LHCII (*29*−*31*). Furthermore, in response to the light-induced phosphorylation of thylakoids, TSP9 can undergo redox-controlled phosphorylation at three threonine sites (T46, T53, and T60) (*21*, *27*). As a consequence, a portion of the phosphorylated TSP9 is released from the thylakoid membrane to the chloroplast stroma (*21*, *27*). It has been demonstrated that the dissociation of TSP9 from the thylakoid membrane can also be driven by high salt and/or low detergent (*30*).

Sequence analysis shows that TSP9 has a high isoelectric point (pI = 9.8) and low sequence complexity, predominantly because of its high Gly (18%), Lys (18%), Ser (10%), and Thr (10%) content (Supporting Information, Figure S1). TSP9 is mostly disordered as predicted by PSIPRED (*32*), DisEMBL (*33*), and PONDR (*34*) programs. The most notable structural feature of TSP9, as predicted from the PSIPRED server, is a short N-terminal α-helix (Supporting Information, Figure S1).

The predicted intrinsic disorder of TSP9, its unique membrane association property, and the proposed role of phosphorylation in its function prompted the following questions. Is the protein disordered in solution as predicted, and does the structure of the protein change upon phosphorylation or association with the membrane? If so, can the structural properties of TSP9 provide clues to the physiological role? As an approach to these questions, we have investigated the structural and dynamic features of TSP9 in both aqueous solution and membrane environment.

In this study, we used NMR spectroscopy to identify the structural features of spinach TSP9 and a mimic of its triphosphorylated form TSP9(T43E+T53E+T60E) in aqueous solution and in micelles. Both TSP9 and the triple mutant were found to be dynamically disordered in aqueous solution, but TSP9 becomes partially structured in a membrane-mimetic environment (either SDS or DPC micelles). We determined the solution structure and backbone dynamics of TSP9 in SDS micelles and deduced the position of TSP9 in SDS micelles from the combined analysis of the intermolecular NOEs between TSP9 and SDS molecules and spin-probe induced NMR signal broadenings. On the basis of these results, we present a model for the phosphorylation-modulated membrane association of TSP9 that can be tested by further experiments.

EXPERIMENTAL PROCEDURES

Protein Production and Labeling. The cDNA coding for mature spinach TSP9 was obtained by PCR as described (*21*). The gene for mature TSP9 was initially cloned into a pUNI vector (*35*, *36*) by in vivo recombination and subsequently N-terminally fused to a construct containing maltose binding protein (MBP), a His_6- affinity tag, and a protease cleavage site. The triple mutant, TSP9(T43E+T53E+T60E), was constructed by site-directed mutagenesis. The numbering system used here is that of the native, mature sequence of TSP9. These constructs were transferred into the pVP13 vector (developed in house) and transformed into Rosetta2-(DE3)/pLysS (Novagen) host cells. Stable-isotope-labeled protein for NMR studies was produced from a ^{15}N- or $^{15}N/^{13}C$-enriched medium according to an established protocol (*37*). The cells were harvested by centrifugation and stored overnight at −20 °C. The cell pellet was suspended in 50 mL of buffer A (50 mM Na_2HPO_4, 300 mM NaCl, pH 7.5) and sonicated on ice until a very low viscosity of the suspension was achieved. After centrifugation, the supernatant was loaded onto a precharged nickel nitrilotriacetic acid (Ni-NTA) affinity column (QIAGEN) with equilibrated resin. After the column was washed with buffer B (50 mM Na_2HPO_4, 300 mM NaCl, 25 mM imidazole, pH 7.5), the protein was eluted with buffer C (50 mM Na_2HPO_4, 300 mM NaCl, 250 mM imidazole, pH 7.5) and concentrated with an Amicon ultrafiltration device (Amersham Pharmacia, Inc.). The sample was then mixed with His_6-tagged tobacco etch virus (TEV) protease (prepared in house) (1/100, w/w, protease/fusion protein) and dialyzed at 25 °C against the TEV reaction buffer (50 mM Tris, 0.5 mM DTT, pH 8.0). After cleavage, the protein mixture was exchanged into buffer A prior to being applied to a Ni-NTA column. The target protein was collected from the column flow-through, and ultrafiltration was used to concentrate the protein and to exchange it into the NMR buffer. The 84-residue protein product (wild type TSP9 or the mutant) included a non-native N-terminal serine left after TEV cleavage. The protein purity (>95%) was determined by SDS−PAGE. The protein yields per liter of culture generally were 1−2 mg of [U-^{13}C,^{15}N]-TSP9, 5 mg of [U-^{15}N]-TSP9 (either wild type TSP9 or the mutant).

NMR Data Collection and Analysis. For the NMR studies in the absence of detergent micelles, [U-^{15}N]-TSP9 variants were dissolved in the NMR buffer containing 90% H_2O/10% D_2O, 10 mM HEPES, 100 mM NaCl, pH 7.0. For the NMR structural studies in the presence of SDS, [U-^{15}N]- or [U-^{13}C,^{15}N]-TSP9 was dissolved in the NMR buffer containing 90% H_2O/10% D_2O, 10 mM HEPES, 100 mM NaCl, and 75 mM SDS micelles, pH 7.0.

All NMR spectra were recorded at the National Magnetic Resonance Facility at Madison (NMRFAM) on a Varian Inova (600 MHz) spectrometer or on Bruker (600 and 750 MHz) spectrometers each equipped with a triple-resonance CryoProbe. The temperature of each sample was regulated at 25 °C. For chemical shift assignment and structure determination, a series of 2D and 3D heteronuclear NMR spectra were collected with a sample of 0.5 mM [U-^{13}C,^{15}N]-TSP9 dissolved in buffer containing SDS: 2D $^1H-^{15}N$ HSQC, 2D $^1H-^{13}C$ HSQC, HNCACB, CBCA(CO)NH, HNCO, HCCONH, CCONH, HCCH-COSY, 3D ^{15}N-edited $^1H-^1H$ NOESY (τ_{mix} = 100 ms), and 3D ^{13}C-edited $^1H-^1H$ NOESY (τ_{mix} = 120 ms). In addition, ^{13}C,^{15}N-filtered/^{13}N-edited $^1H-^1H$ NOESY (τ_{mix} = 100 ms) and 3D ^{13}C,^{15}N-filtered/^{13}C-edited $^1H-^1H$ NOESY (τ_{mix} = 150 ms) data (*38*) were also collected to observe intermolecular NOE signals between TSP9 and SDS molecules. A sample of 0.5 mM [U-^{15}N]-TSP9 in the SDS buffer was used for the collection of steady state $\{^1H\}-^{15}N$ NOE and ^{15}N relaxation (R_1, R_2) data by standard pulse sequences (*39*). To determine the ^{15}N R_1 values, NMR spectra were recorded with delays of 100, 300, 500, 700, 900, 1300, and 1700 ms. To determine ^{15}N R_2 values, NMR spectra were recorded with delays of 10,

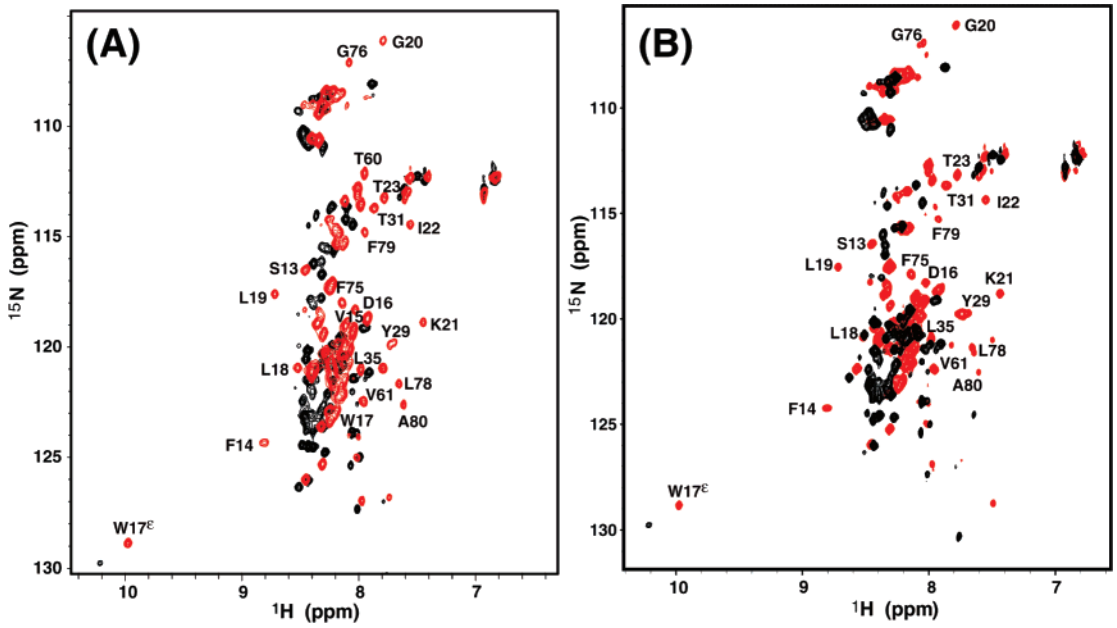

FIGURE 1: (A) ^{1}H−^{15}N HSQC spectra of TSP9 in aqueous solution (peaks in black) and in 75 mM SDS (peaks in red). (B) ^{1}H−^{15}N HSQC spectra of TSP9(T46E+T53E+T60E) in aqueous solution (peaks in black) and in 75 mM SDS (peaks in red). Residues exhibiting significant chemical shift changes on addition of SDS are labeled with their sequence number. The numbering system used here is that of the native, mature sequence of TSP9.

30, 50, 70, 90, 130, and 170 ms. The relaxation rates were calculated by least-squares fitting of peak heights versus relaxation delay to one single-exponential decay. The reported error estimates are standard deviations derived from fitting the data. Steady state {^{1}H}−^{15}N NOE values were calculated from the ratio of peak heights in a pair of NMR spectra acquired with and without proton saturation. The signal-to-noise ratio in each spectrum was used to estimate the experimental uncertainty. To determine the paramagnetic relaxation effects of 5-doxylstearic acid (5-DSA) and 16-doxylstearic acid (16-DSA) (Aldrich) on micelle-bound TSP9, 2D ^{1}H−^{15}N HSQC spectra were collected for 0.2−0.3 mM TSP9 in the absence or presence of 2 mM 5-DSA or 16-DSA. The relaxation enhancement effect for each probe was evaluated by the remaining amplitudes of the peak heights, defined by the ratios of the peak heights in a pair of NMR spectra acquired before and after addition of the paramagnetic probe. The experimental uncertainties were also determined by evaluating the noise level in each spectrum. For the SDS titration experiments, 2D ^{1}H−^{15}N HSQC spectra were collected of 0.2−0.3 mM [U-^{15}N]-TSP9 variants mixed with 0, 1, 2, 4, 8, 16, 50, 100, or 150 mM SDS. For the DPC titration experiments, 2D ^{1}H−^{15}N HSQC spectra were also collected for 0.1−0.2 mM [U-^{15}N]-TSP9 mixed with 0, 0.5, 1, 2, 4, 8, 16, 32, 53, or 100 mM DPC. The translational diffusion coefficient of TSP9 in aqueous solution was determined by a water-suppressed longitudinal encode−decode (Water-SLED) experiment (*40*). The gradient was calibrated by reference to data for 10 mg/mL lysozyme (14.4 kDa), which has a diffusion coefficient of 1.11×10^{-6} cm^2 s^{-1} (*41*).

Spectra were processed and analyzed, respectively, with the NMRPipe (*42*) and Sparky (http://www.cgl.ucsf.edu/home/sparky) software packages. The time-domain NMR data and chemical shift assignments have been deposited in the BioMagResBank database under BMRB accession number 6926.

Distance constraints used in the structure determination were derived from ^{13}C-edited ^{1}H−^{1}H NOESY and ^{15}N-edited ^{1}H−^{1}H NOESY data, and dihedral angle constraints (ϕ and ψ) were determined from assigned chemical shifts submitted to the TALOS (*43*) program. The automated NOE assignment module of Cyana (*44*) was used in generating initial NOE assignments and the initial structural ensemble. The NMR structure was refined further through corrections of NOE assignments and additional Cyana calculations. In the final round of structure calculation, a total of 767 NOE distance constraints and 28 backbone ϕ and ψ constraints were used. The three-dimensional coordinates for 20 structural models representing the structure of TSP9 have been deposited in the Protein Data Bank (PDB) under the accession number 2FFT.

RESULTS

SDS Micelle-Induced Folding of TSP9. Effects of solution conditions on the conformations of TSP9 and TSP9-(T43E+T53E+T60E) were followed by two-dimensional ^{1}H−^{15}N HSQC spectroscopy. As shown in Figure 1A, the resonance peaks in the ^{1}H−^{15}N HSQC spectrum of TSP9 in the buffer without SDS is poorly dispersed with all the peaks along the ^{1}H dimension within the 8.0−8.5 ppm range. A narrow chemical shift dispersion of this type is diagnostic for dynamic disorder. A similar NMR spectral feature was observed for TSP9(T43E+T53E+T60E) (Figure 1B), suggesting that introduction of the negative charges to the phosphorylation sites of TSP9 has no effect on its conformation. The translational diffusion coefficient determined for TSP9 in the buffer without SDS was 1.20×10^{-6} cm^2 s^{-1}, higher than that for the 14.4 kDa lysozyme (1.11×10^{-6} cm^2 s^{-1}); this indicates that TSP9 is mostly monomeric under these conditions. The monomeric state of TSP9 is further supported by gel filtration chromatography results (data not shown).

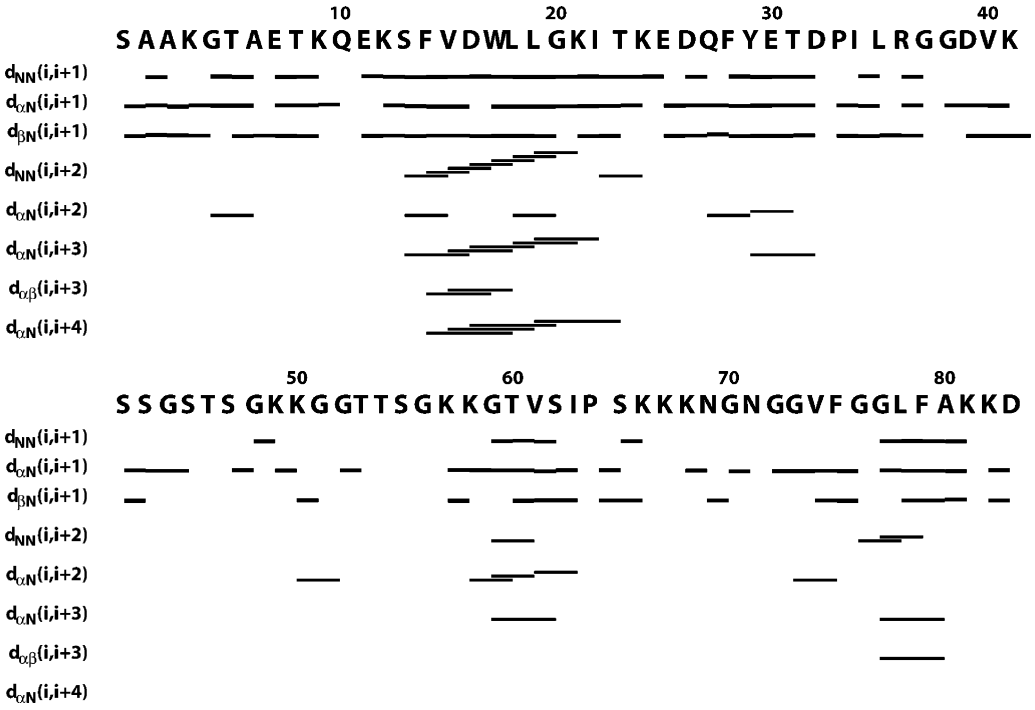

FIGURE 2: Sequential NOE connectivities used in calculating the structure of TSP9.

Because the majority of TSP9 is associated with the thylakoid membrane under the physiological condition, we decided to investigate the conformation of TSP9 in a membrane mimetic environment. We chose SDS micelles on the basis of previous successful applications of this membrane mimicking system to structural characterizations of membrane proteins (*45*−*48*). As shown in Figure 1A,B, extensive changes are observed in the ^{1}H−^{15}N HSQC spectra of both TSP9 and TSP9(T43E+T53E+T60E) in the presence of 75 mM SDS micelles. Compared to those of free TSP9 variants, the NMR spectra of TSP9 variants in SDS micelles display much broader chemical shift dispersion; this suggests that the TSP9 variants undergo a folding transition in the presence of SDS micelles. A number of peaks, including that from the Nϵ1 group of W17, are shifted significantly either to lower or higher frequencies in the ^{1}H dimension. The improved spectral resolution made it possible to determine sequence-specific chemical shift assignments for TSP9 in SDS micelles. The assigned chemical shifts reveal that the residues subject to micelle-induced folding are mainly located in four regions of the sequence: F14−K24 (near the N-terminus), Y29−R36, T60−V61, and G73-A80 (near the C-terminus) (Figure 1A). For example, the chemical shifts of 0.6 ppm for the signals assigned to K21 H$^{\gamma 2}$ and to V74 H$^{\gamma 2}$ suggest that the environments of these residues become ordered in the presence of SDS.

Although no long-range NOEs indicative of a stable tertiary fold were observed, it was possible to determine regions of secondary structure in TSP9 in SDS micelles (Figure 2). As shown in Figure 3, the most distinct structural feature of TSP9 is the α-helix formed by residues F14−T23 (α_1), with a backbone r.m.s.d. of 0.33 Å. Detailed analysis of the α_1-helix further revealed that it does not show distinct amphipathic characteristics: hydrophobic side chains are located on almost every face of the helix (Figure 3B). A second prominent structural feature is the less convergent α-helical turn formed by C-terminal residues F75−F79 (α_2),

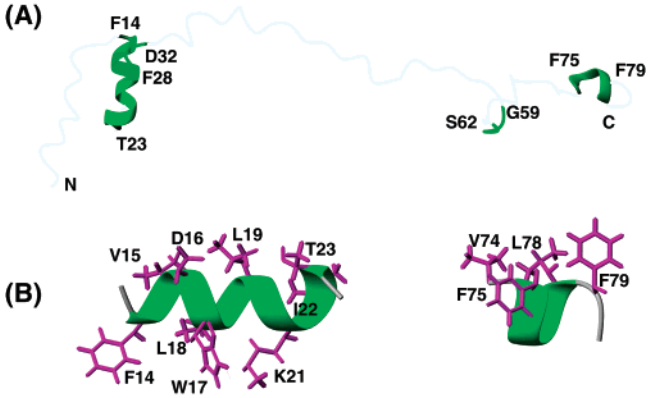

FIGURE 3: Solution structure of TSP9 in SDS micelles. (A) Ribbon representation of the whole TSP9 molecule. The α_1, α_2, and residues F28−D32 and G59−S62, which show the $d_{\alpha N}(i,i+2)$ NOE connectivities, are green. The structurally disordered regions are shown in light gray. (B) Representation of the two helical structural elements. The figure was made with MOLMOL (*75*).

with a backbone r.m.s.d. of 1.0 Å. This short helical turn contains two adjacent glycines (G76 and G77). As a result, nearly all the bulky hydrophobic chains are clustered on one face of the helix (Figure 3B). In addition to the α_1-helix and α_2-helical turn, a few $d_{\alpha N}(i,i+2)$ and $d_{\alpha N}(i,i+3)$ NOE connectivities observed for residues F28−D32 and G59−S62 (Figure 2) suggested that these residues become ordered in the presence of SDS micelles. These structural elements are dominated by hydrophobic residues (Figure 4A) that appear to favor the hydrophobic environment of the micelles.

Interaction between TSP9 and SDS Micelles. ^{1}H−^{1}H NOEs between [^{13}C,^{15}N]-TSP9 and unlabeled SDS molecules were identified from analysis of ^{13}C,^{15}N-filtered/^{13}C-edited ^{1}H−^{1}H NOESY and ^{13}C,^{15}N-filtered/^{15}N-edited ^{1}H−^{1}H NOESY experiments. The intense ^{1}H NMR signals from the aliphatic chains of SDS were assigned as follows: δ_{C1-H} (4.0 ppm), δ_{C2-H} (1.67 ppm), δ_{C3-11H} (1.22−1.37 ppm), and δ_{C12-H} (0.88 ppm). The NOEs identified residues of TSP9

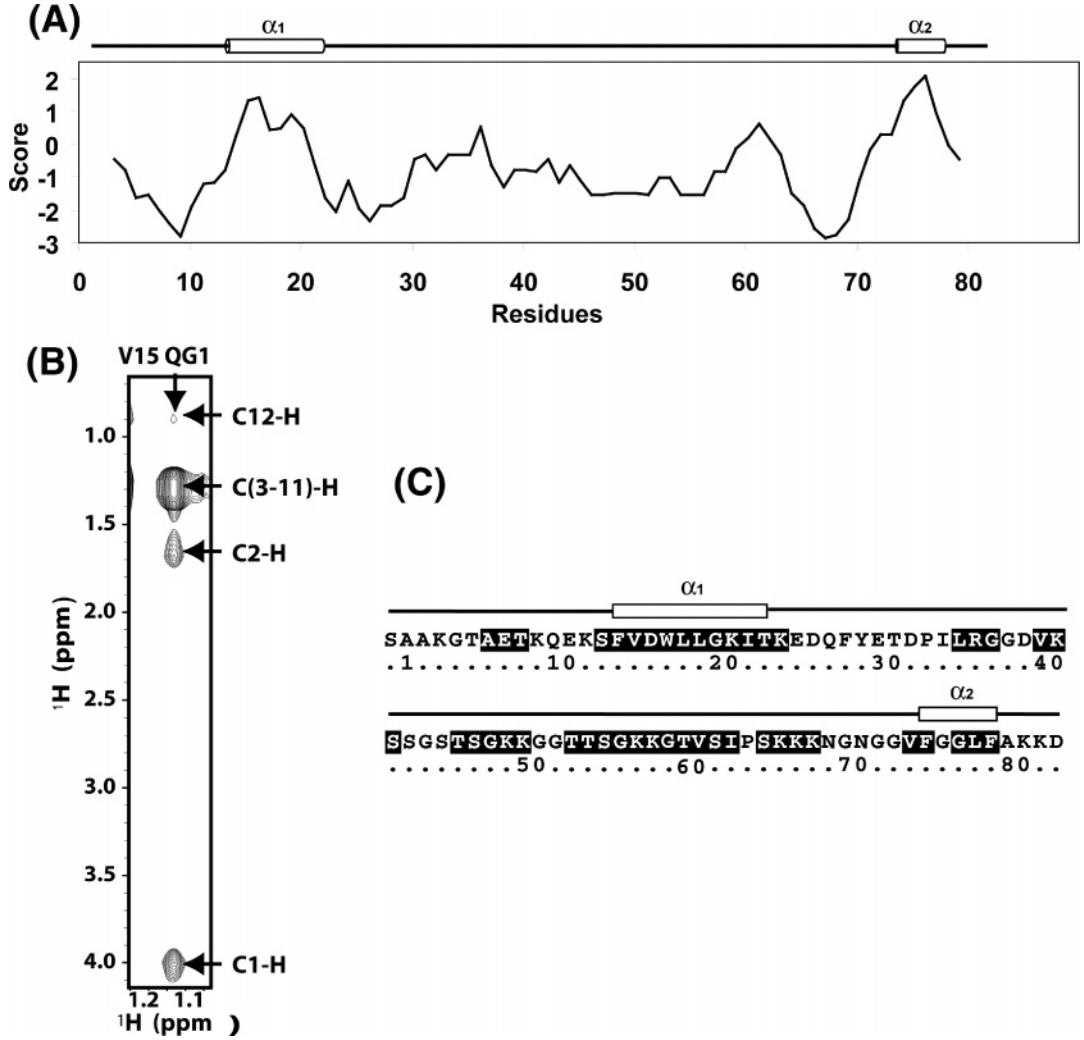

FIGURE 4: (A) Kyte−Doolittle hydropathy plot (*76*) of TSP9. (B) Selected region of the $^{15}N,^{13}C$-filtered/^{13}C-edited $^{1}H,^{1}H$-NOESY of TSP9 in SDS micelles, highlighting the NOE signals between the H^{γ} atoms (QG1) of Val15 (top) and the atoms of SDS molecules (right, C-1H). (C) Residues of TSP9 that show NOEs with SDS micelles are highlighted in dark in the amino acid sequence.

that are spatially close to the micelles (Figure 4B,C). When mapped to the structure of TSP9, these residues are located in both the structured regions (α_1- and α_2-helices) and unstructured regions (Figure 4C), including the segment (L35−K68) where the three phosphorylation sites are located. Regions lacking appreciable NOEs with SDS also are spread over the primary sequence of TSP9.

To determine the nature of the interaction between TSP9 and SDS, 2D $^{1}H-^{15}N$ HSQC spectra were collected for [U-^{15}N]-TSP9 mixed with 0, 1, 2, 4, 8, 16, 50, 100, and 150 mM SDS. Whereas the NMR signal of the Nϵ1 group of Trp17 shifted upfield continuously with addition of SDS, folding transition was observed between 8 and 16 mM SDS (data not shown). This concentration of SDS is beyond the critical micelle concentration (CMC) of SDS and is equivalent to 0.1−0.2 mM SDS micelles (*49*). Increasing the SDS concentration from 16 mM to 150 mM SDS did not lead to appreciable additional spectral changes. These observations suggest that TSP9 interacts with individual SDS molecules, but the folding of TSP9 is only induced by the SDS micelles. The effect was confirmed by titrating TSP9 with 0, 0.5, 1, 2, 4, 8, 16, 32, 53, or 100 mM DPC; TSP9 in DPC micelles was found to adopt a folded conformation similar to that in SDS micelles (Supporting Information, Figure S2). Further evaluation of the NMR signals (e.g., that of the Nϵ1 group of W17) reveals that binding of TSP9 to DPC only occurred when DPC reached 2 mM or higher, beyond the CMC of DPC (*49*); and the folded conformation of TSP9 was finally stabilized at 8 mM DPC (data not shown). Together, these results suggest that the folding of TSP9 can be induced in both SDS and DPC micelles. In addition, the cationic property of TSP9 also allows it to associate with individual SDS molecules in a noncooperative manner, as observed for other cationic peptides (*47*).

Positioning of TSP9 in SDS Micelles. The insertion of TSP9 in SDS micelles was investigated by the paramagnetic effect of two spin-labeled stearates, 5-DSA and 16-DSA. These two compounds, through the unpaired electron in the nitroxide, can accelerate the relaxation of neighboring nuclear spins via dipole−dipole interactions. They also have high tendency to penetrate into the micelles, with 5-DSA localized at the interfacial regions and 16-DSA at the interior sites respectively (*51*). Thus, the paramagnetic effect from these two spin-labels has been widely used to probe the insertion depth of proteins or peptides in micelles (*52*−*56*).

2D $^{1}H-^{15}N$ HSQC spectra were collected for TSP9 before and after addition of either 5-DSA or 16-DSA, and the remaining amplitudes of NMR signals were computed as

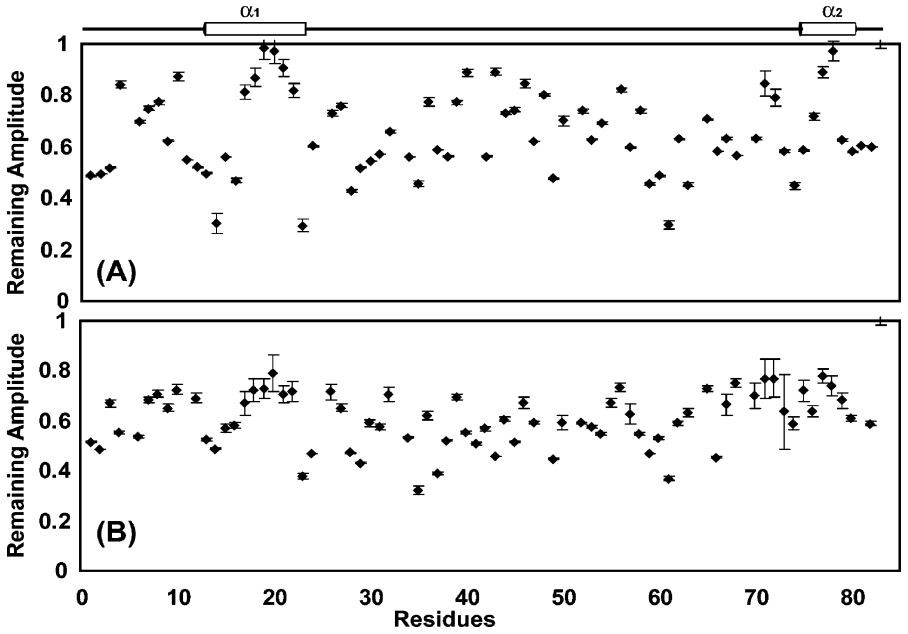

FIGURE 5: Paramagnetic relaxation of TSP9 induced by nitroxide radicals. (A) Remaining amplitude of the amide peaks of TSP9 after the addition of 5-DSA. (B) Remaining amplitude of the amide peaks of TSP9 after the addition of 16-DSA.

ratios of peak heights between two spectra. As shown in Figure 5A, the presence of 5-DSA results in significant reductions in peak intensities for the majority of residues in TSP9, supporting extensive contact between TSP9 and the micelle. These affected residues are spread over both the structured region (α_1-helix) and the disordered regions, including the regions containing the potential phosphorylation sites and the N- and C-termini (A1−K3, A80−K82). However, the C terminal D83 is unaffected. Furthermore, the effect of 5-DSA on the α_1-helix decreases gradually along the chain from F14 to L19 and then increases again from G20 to T23. The gradual change of sensitivity to the paramagnetic probe implicates the progressive immersion of the residues of F14−L19 in the micelle, but the turning point at position 20 may also suggest the existence of a curvature in that part of the helix. In addition, the signal reductions of the short α_2-helical turn also show a gradual increment from F75 to L78. The paramagnetic effect of 16-DSA is similar to that of 5-DSA (Figure 5B). The regions affected by the two paramagnetic probes are nearly the same, suggesting that the insertion of the TSP9 segments in the micelle may be shallow. In particular, the site-dependent signal reductions observed for residues in α_1 and α_2 in the presence of 5-DSA are also observed in the presence of 16-DSA.

Although the NMR signal of the backbone amide group of W17 is only slightly affected by the paramagnetic probes, its side-chain Nϵ1 group shows a remarkable signal reduction: 0.36 in the presence of 5-DSA and 0.49 in the presence of 16-DSA. Thus, the indole ring of W17 very likely is anchored in the micelle.

Backbone Dynamics of TSP9 in SDS Micelles. The backbone dynamics of TSP9 in SDS micelles was investigated by measuring the ^{15}N relaxation rates R_1 and R_2 as well as the steady state $\{^1H\}$-^{15}N NOE at the field strength of 14.1 T (600 MHz ^{1}H). These parameters are influenced by the molecular tumbling time and by local motions on the pico- to nanosecond time scale. In addition, R_2 is also sensitive to slow chemical exchange on the micro- to millisecond time scale.

The R_1, R_2, and $\{^1H\}-^{15}N$ NOE values for TSP9 in the SDS micelles are reported in Figure 6. From the average heteronuclear NOE value of 0.32, it is evident that TSP9 in SDS micelles retains high flexibility. Nevertheless, different regions of the molecule exhibit distinct dynamic behavior. The regions with the greatest mobility are the N-terminus, up to approximately residue Q10, and the C-terminus (A80−D83). These two regions have comparatively lower R_2 and NOE values but relatively higher R_1 values. Three residues in these terminal regions (A1, K82, and D83) exhibited negative $\{^1H\}-^{15}N$ NOE values. The region with the second highest mobility, K24−F79, includes the α_2-helical turn. This region has an average NOE value of 0.19, indicative of high dynamic disorder. The R_1 values of residues in the α_2-helical turn are similar to those in the termini, but the R_2 values are higher. Note that, although the residues in the α_2-helical turn are structured, their NOE values are only slightly higher than the average. The most structured region is the α_1-helix with NOE values (0.58−0.67) well above the average. Consistent with the NOE observations, the R_2 values for these helical residues are significantly higher than those for the rest of TSP9, while the R_1 values are lower. Interestingly, even the residues within the α_1-helix exhibit variation in backbone dynamics. For example, residues at the two ends of the α_1-helix show appreciably higher R_2 and NOE values and lower R_1 values than central residues D16 and L18 (peak overlap prevented relaxation measurements for W17). The origin of the greater dynamics of the central residues of the α_1-helix remains to be investigated.

The high internal mobility of TSP9 prevented the determination of its overall molecular tumbling time (τ_m) from R_2/R_1 ratios. However, the average R_2/R_1 ratio of 15.8 determined for residues in the α_1-helix is in good agreement with values found by others for small peptides in SDS micelles at this field strength (*52*, *57*−*58*).

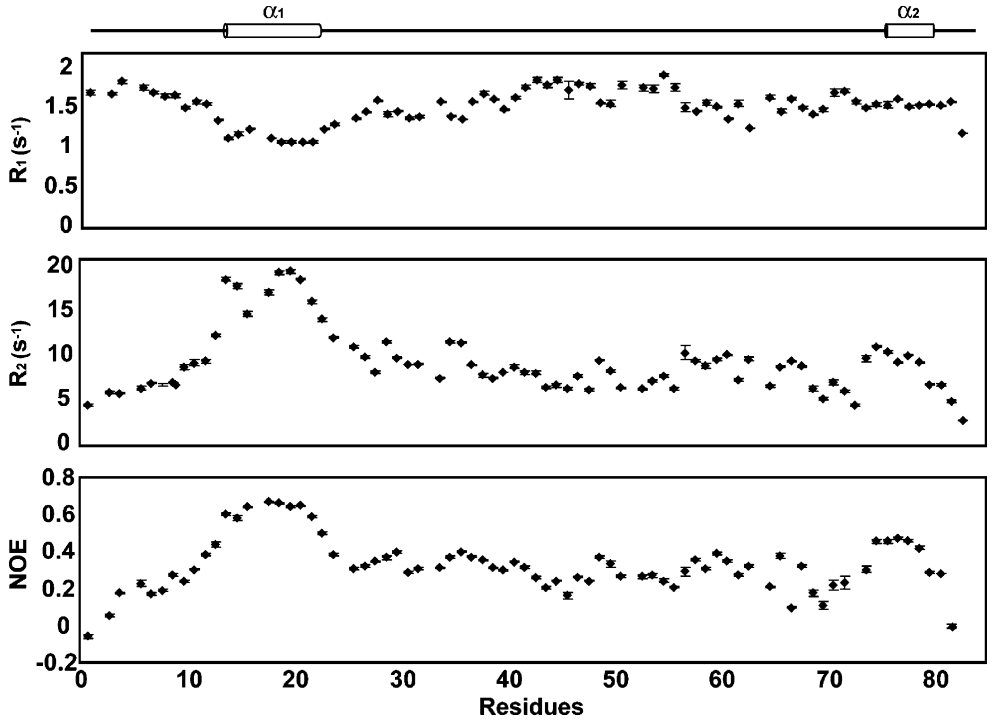

FIGURE 6: Backbone ^{15}N R_1, R_2 relaxation parameters and $^1H-^{15}N$ NOEs of TSP9 in SDS micelles.

DISCUSSION

Micelle-Induced Ordering of TSP9. The NMR spectroscopic studies reported here revealed that TSP9 is unstructured in aqueous solution but becomes partially ordered when bound to an SDS or DPC micelle, a mimic of a membrane surface. The presence of either detergent micelle (SDS or DPC) induced a similar conformation in TSP9. The major structural features of TSP9 in SDS micelles include an N-terminal α-helix and a C-terminal helical turn. In addition, secondary chemical shifts and sequential $d_{\alpha N}(i,i+2)$ and $d_{\alpha N}(i,i+3)$ NOE connectivities observed for residues F28−D32 and G59−S62 suggest that these regions are at least partially ordered. The structured elements of TSP9 contain mainly hydrophobic residues. Thus their structures in SDS micelles are likely induced by the hydrophobic environment inside the micelles. Residues in other regions are disordered and remain so even in the presence of SDS micelles. Because SDS and DPC micelles have been serving as good membrane mimics, the disorder-to-order conformational transition of TSP9 upon association with micelles may have significant physiological relevance.

Over the years, the unique structure−function paradigm displayed by intrinsically disordered proteins has started to gain more attention. Despite their lack of a globular structure, intrinsically disordered proteins play key roles in signal transduction and other critical cellular processes (*59*−*61*). Biochemical and biophysical characterizations of these unstructured proteins have revealed that residual structure, including permanent or transient secondary structural elements, can be present in these proteins and function as protein recognition motifs (*62*). Stabilization of the residual structure is often coupled with other activities: some unstructured proteins and peptides become folded upon binding to their biological targets (*60*, *63*, *64*); others are unfolded under aqueous conditions but fold in the presence of lipids or model membranes (*65*−*67*). Thermodynamically, the induced-folding process is always accompanied by significant entropy−enthalpy compensation. It is believed that the physiological importance of the residual structure is to facilitate molecular recognition during protein−protein interaction (*62*), and the induced folding allows fine control over binding affinity (*63*). For TSP9, it is also possible that the micelle-induced folding controls its functional specificity in the thylakoid membrane.

Position of TSP9 in SDS Micelles. On the basis of NOE signals between the SDS micelles and TSP9, the spin probe-induced broadening of NMR signals, and the observed distribution of backbone dynamics, we have determined protein−micelle contacts on a per residue basis and further inferred the positioning of each residue of TSP9 in SDS micelles. Our NOE observations indicate that the contact between TSP9 and SDS micelles is extensive, in that both the structured regions (α_1- and α_2-helices) and the unstructured regions (including the three phosphorylation sites) show intermolecular NOEs with SDS micelles (Figure 4C). In agreement with this, the addition of paramagnetic probes to the micelle reduced the intensities of NMR signals from residues both in structured and unstructured regions of the protein. As was observed for helical residues 85−99 of membrane associated α-synuclein (*52*), the paramagnetic effects were progressive. In α_1-helix of TSP9, the broadening decreased in the stretch F14−19 and then increased over G20−T23. These results suggest that a kink in the helix may occur at G20 that causes the center of the helix to extend out of the micelle. The α_2-helix also showed progressive broadening effects indicating that the N-terminal part is inserted in the micelle whereas the C-terminal part is anchored at the surface. To confirm this topology, it would be useful to have information from side chains as well as the backbone. For the one residue with side chain information (W17) the results showed much larger intensity reduction for the side chain than for the backbone. The N-terminus (A1−K3) exhibits high sensitivity to micelle-bound spin

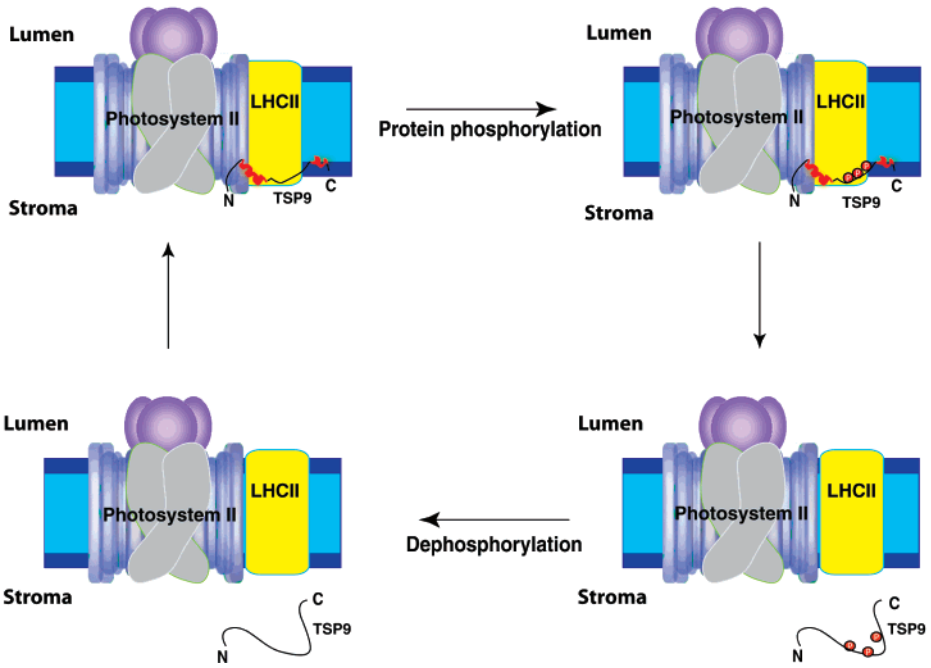

FIGURE 7: Model for the phosphorylation-modulated reversible membrane association of TSP9. The thylakoid membrane is shown by the blue rectangle, and the border in dark blue represents the polar groups of the lipids. The multisubunit PSII complex is represented by the gray (core) and purple blocks, and LHCII is represented by yellow blocks. Phosphorylated threonines are represented by the letter "P" in a red circle.

probes as well as high local mobility, leading to a conclusion that it may be free to move inside the micelle. On the other hand, the highly mobile C-terminal D83 is not affected by the paramagnetic agents, indicating its exposure to the bulk solvent.

Functional Implications of the Interaction between TSP9 and SDS Micelles. The present study has identified several structural elements present in TSP9 in SDS micelles. Of these, the most prominent is the α_1-helix. The idea of a functional role for the α_1-helix is reinforced by examination of the sequence alignment of TSP9 proteins from 44 species (Supporting Information, Figure S3). Although TSP9 sequences from various species are quite divergent, the α_1-helix is one of the most conserved regions in the protein. When TSP9 was first identified, because it was the only soluble protein undergoing light-induced phosphorylation in the thylakoid membrane, it was considered as a candidate signaling factor for regulating redox-controlled gene expression (*21*, *27*). However, the structural features of TSP9 do not resemble those of any identified transcription factor. Although the protein has a region enriched with basic residues, this part of the molecule is disordered. Therefore, we suggest that the physiological function of TSP9 is not directly related to the regulation of gene expression.

The observation of interactions between the unstructured regions of TSP9 and SDS micelles suggests that these disordered regions may play a role in modulating the membrane association of TSP9. Conceivably, the large number of lysines in these regions may facilitate the attachment of TSP9 to the negatively charged membrane. Furthermore, the three phosphorylation sites (T46, T53, and T60) are also located in the unstructured region and make contacts with SDS micelles. Thus, it is reasonable to assume that phosphorylation of these sites will lower the membrane association affinity of TSP9. Indeed, it has been shown that phosphorylation of TSP9 can cause 15% to 25% of the protein to dissociate from thylakoid membrane (*21*). Additionally, when binding to individual SDS molecules, significant exchange broadening of NMR signals was observed for TSP9(T43E+T53E+T60E), but not wild type TSP9 (data not shown), consistent with the observation that introduction of negative charges to TSP lowered its membrane association affinity.

Localization of TSP9 in the protein complexes from thylakoid membrane and analysis of TSP9 cross-linking with the proteins of spinach thylakoids provide several lines of experimental evidence for association of TSP9 with LHCII and its localization at the interface between PSII and LHCII (Hansson, M., Vener, A.V., Carlberg, I., unpublished data). The structure of TSP9 is related to its membrane association and could be important for its interaction with the PSII−LHCII supercomplex. Thus far, a structure of PSII−LHCII supercomplex is only available at low resolution (*68*, *69*). Nevertheless, a few of the minor Lhcb (light harvesting chlorophyll *a*/*b*-binding proteins of photosystem II) polypeptides, particularly CP29, have been shown to stabilize the supercomplex of PSII and LHCII (*70*), probably through helical contacts (*71*). In response to light- and redox-regulated phosphorylation, a fraction of LHCII migrates from PSII to PSI. The molecular mechanism for this step called the state transition remains unclear (*18*). However, the recent structural and biochemical studies of state transitions in green alga *Chlamydomonas reinhardtii* revealed that multiple differential phosphorylation of CP29, the linker protein coupling LHCII to the PSII core, is an essential part of state transitions (*71*−*73*). In reducing conditions CP29 becomes phosphorylated at four distinct residues in its N-terminus and together with LHCII migrates from PSII to PSI (*72*, *74*). The multiple light and redox dependent phosphorylation of CP29 is specific for green alga (*74*) because in plants CP29 was found only singly phosphorylated (*15*). Thus, the multiple light-dependent phosphorylation of plant-specific TSP9, which is

like CP29 localized at the interface between the the PSII core and LHCII, could be involved in regulation of light harvesting in plants. Our current study on the structure of TSP9 in SDS micelles may provide additional insight into the process of TSP9 binding to the thylakoid membrane. Because TSP9, as implied by its mapped location in the thylakoid membrane, may interact with both PSII and LHCII through its helical structure, it is an intriguing possibility that the phosphorylation-dependent dissociation of TSP9 from the membrane contributes to the state transitions and the association of LHCII with the photosystems.

On the basis of our knowledge of the micelle-induced folding of TSP9 and the close relation between TSP9 and the PSII−LHCII supercomplex, as well as the assumption of the phosphorylation-modulated membrane association, we propose a structural model for the phosphorylation-modulated association of TSP9 with thylakoid membrane (Figure 7). In this model, nonphosphorylated TSP9 is anchored to the membrane through both its structured and unstructured regions. The α_1-helix, the most notable structural element in TSP9, is the potential primary functional site of interaction between TSP9 and the neighboring PSII and LHCII in the thylakoid membrane. Upon phosphorylation of the three threonines in the unstructured region of TSP9, the interaction between TSP9 and the membrane becomes weakened by electrostatic repulsion. Consequently, a fraction of TSP9 molecules migrate to the aqueous stroma solution. Because the state transitions occur coincidently, it can be imagined that the dissociation of TSP9 from the membrane may also contribute to the disruption of the PSII−LHCII supercomplex. In stroma, TSP9 becomes completely unstructured, with its phosphorylated sites exposed. The phosphate groups of TSP9 are eventually removed by the phosphatase in solution, leading to the return of TSP9 to the membrane. This model presents a novel role for the unstructured segments and their phosphorylation in regulating the biological function of the proteins. However, because the relationship between TSP9 and PSII−LHCII supercomplex is not well established, and the fate of the TSP9 in stroma solution is unknown, our proposed model requires additional experimental validation. The proposed structural model of TSP9 can be tested by further study of the interaction between TSP9 and PSII or LHCII, as well as by investigating the physiological consequences of TSP9 mutants.

ACKNOWLEDGMENT

The authors thank Dr. Deborah Berthold for her advice on preparing the initial construct for overexpression of TSP9 and the many team members from the Center for Eukaryotic Structural Genomics who provided excellent infrastructure for this work.

SUPPORTING INFORMATION AVAILABLE

Figure S1 showing secondary structural elements predicted from the PSIPRED program, Figure S2 with the $^{1}H-^{15}N$ HSQC spectrum of TSP9 in 100 mM DPC at pH 7.0, and Figure S3 with the multiple sequence alignment of TSP9 proteins from 44 species. This material is available free of charge via the Internet at http://pubs.acs.org.

REFERENCES

1. Barber, J. (2002) Photosystem II: a multisubunit membrane protein that oxidises water, *Curr. Opin. Struct. Biol. 12*, 523−530.
2. Nelson, N., and Yocum, C. F. (2006) Structure and Function of Photosystems I and II, *Annu. Rev. Plant Biol. 57*, 521−565.
3. Grossman, A. R., Bhaya, D., Apt, K. E., and Kehoe, D. M. (1995) Light-harvesting complexes in oxygenic photosynthesis: diversity, control, and evolution, *Annu. Rev. Genet. 29*, 231−288.
4. Allen, J. F., Bennett, J., Steinback, K. E., and Arntzen, C. J. (1981) Chloroplast protein phosphorylation couples plastoquinone redox state to distribution of excitation energy between photosystems, *Nature 291*, 25−29.
5. Vener, A. V., Ohad, I., and Andersson, B. (1998) Protein phosphorylation and redox sensing in chloroplast thylakoids, *Curr. Opin. Plant Biol. 1*, 217−223.
6. Vener, A. V., van Kan, P. J., Rich, P. R., Ohad, I., I, and Andersson, B. (1997) Plastoquinol at the quinol oxidation site of reduced cytochrome *bf* mediates signal transduction between light and protein phosphorylation: Thylakoid protein kinase deactivation by a single-turnover flash, *Proc. Natl. Acad. Sci. U.S.A. 94*, 1585−1590.
7. Zito, F., Finazzi, G., Delosme, R., Nitschke, W., Picot, D., and Wollman, F. A. (1999) The Qo site of cytochrome *b6f* complexes controls the activation of the LHCII kinase, *EMBO J. 18*, 2961−2969.
8. Snyders, S., and Kohorn, B. D. (1999) TAKs, thylakoid membrane protein kinases associated with energy transduction, *J. Biol. Chem. 274*, 9137−9140.
9. Snyders, S., and Kohorn, B. D. (2001) Disruption of thylakoid-associated kinase 1 leads to alteration of light harvesting in *Arabidopsis*, *J. Biol. Chem. 276*, 32169−32176.
10. Bellafiore, S., Barneche, F., Peltier, G., and Rochaix, J. D. (2005) State transitions and light adaptation require chloroplast thylakoid protein kinase STN7, *Nature 433*, 892−895.
11. Vainonen, J. P., Hansson, M., and Vener, A. V. (2005) STN8 protein kinase in *Arabidopsis thaliana* is specific in phosphorylation of photosystem II core proteins, *J. Biol. Chem. 280*, 33679−33686.
12. Silverstein, T., Cheng, L., and Allen, J. F. (1993) Chloroplast thylakoid protein phosphatase reactions are redox-independent and kinetically heterogeneous, *FEBS Lett. 334*, 101−105.
13. Testi, M. G., Croce, R., Polverino-De Laureto, P., and Bassi, R. (1996) A CK2 site is reversibly phosphorylated in the photosystem II subunit CP29, *FEBS Lett. 399*, 245−250.
14. Vener, A. V., Harms, A., Sussman, M. R., and Vierstra, R. D. (2001) Mass spectrometric resolution of reversible protein phosphorylation in photosynthetic membranes of *Arabidopsis thaliana*, *J. Biol.Chem. 276*, 6959−6966.
15. Hansson, M., and Vener, A. V. (2003) Identification of three previously unknown in vivo protein phosphorylation sites in thylakoid membranes of *Arabidopsis thaliana*, *Mol. Cell Proteomics 2*, 550−559.
16. Lunde, C., Jensen, P. E., Haldrup, A., Knoetzel, J., and Scheller, H. V. (2000) The PSI-H subunit of photosystem I is essential for state transitions in plant photosynthesis, *Nature 408*, 613−615.
17. Haldrup, A., Jensen, P. E., Lunde, C., and Scheller, H. V. (2001) Balance of power: a view of the mechanism of photosynthetic state transitions, *Trends Plant Sci. 6*, 301−305.
18. Allen, J. F., and Forsberg, J. (2001) Molecular recognition in thylakoid structure and function, *Trends Plant Sci. 6*, 317−326.
19. Allen, J. F. (1983) Protein phosphorylation−Carburettor of photosynthesis?, *Trends Biochem. Sci. 8*, 369−373.
20. Bennett, J. (1983) Regulation of photosynthesis by reversible phosphorylation of the light-harvesting chlorophyll *a*/*b* protein, *Biochem. J. 212*, 1−13.
21. Carlberg, I., Hansson, M., Kieselbach, T., Schroder, W. P., Andersson, B., and Vener, A. V. (2003) A novel plant protein undergoing light-induced phosphorylation and release from the photosynthetic thylakoid membranes, *Proc. Natl. Acad. Sci. U.S.A. 100*, 757−762.
22. Hammer, M. F., Markwell, J., and Sarath, G. (1997) Purification of a protein phosphatase from chloroplast stroma capable of dephosphorylating the light-harvesting complex-II, *Plant Physiol. 113*, 227−233.
23. Andersson, B., and Aro, E.-M. (1997) Proteolytic activities and proteases of plant chloroplasts, *Physiol. Plant. 100*, 780−793.
24. Michel, H., Hunt, D. F., Shabanowitz, J., and Bennett, J. (1988) Tandem mass spectrometry reveals that three photosystem II

proteins of spinach chloroplasts contain N-acetyl-O-phosphothreonine at their NH2 termini, *J. Biol. Chem. 263*, 1123−1130.
25. Michel, H. P., and Bennett, J. (1987) Identification of the phosphorylation site of an 8.3 kDa protein from photosystem II of spinach, *FEBS Lett. 212*, 103−108.
26. Rintamäki, E., and Aro, E.-M. (2001) *Regulation of Photosynthesis*, Kluwer, Dordrecht, The Netherlands.
27. Bhalla, P., and Bennett, J. (1987) Chloroplast phosphoproteins: phosphorylation of a 12-kDa stromal protein by the redox-controlled kinase of thylakoid membranes, *Arch. Biochem. Biophys. 252*, 97−104.
28. Hansson, M., Dupuis, T., Strömquist, R., Andersson, B., Vener, A. V., and Carlberg, I. (2006) The mobile thylakoid phosphoprotein TSP9 interacts with the light harvesting complex II and the peripheries of both photosystems, unpublished
29. Lindahl, M., Carlberg, I., Schröder, W. P., and Andersson, B. (1995) *Photosynthesis: From Light to Biosphere*, Kluwer, Dordrecht, The Netherlands.
30. Carlberg, I., and Andersson, B. (1996) Phosphatase activities in spinach thylakoid membranes-effectors, regulation and location, *Photosynth. Res. 47*, 145−156.
31. Bennett, J., Shaw, E. K., and Bakr, S. (1987) Phosphorylation of thylakoid proteins and synthetic peptide analogs : Differential sensitivity to inhibition by a plastoquinone antagonist, *FEBS Lett. 210*, 22−26.
32. McGuffin, L. J., Bryson, K., and Jones, D. T. (2000) The PSIPRED protein structure prediction server, *Bioinformatics 16*, 404−405.
33. Linding, R., Jensen, L. J., Diella, F., Bork, P., Gibson, T. J., and Russell, R. B. (2003) Protein disorder prediction: implications for structural proteomics, *Structure 11*, 1453−1459.
34. Li, X., Romero, P., Rani, M., Dunker, A. K., and Obradovic, Z. (1999) Predicting Protein Disorder for N-, C-, and Internal Regions, *Genome Inform. Ser. Workshop Genome Inform. 10*, 30−40.
35. Liu, Q., Li, M. Z., Liu, D., and Elledge, S. J. (2000) Rapid construction of recombinant DNA by the univector plasmid-fusion system, *Methods Enzymol. 328*, 530−549.
36. Berthold, D. A., Stenmark, P., and Nordlund, P. (2003) Screening for functional expression and overexpression of a family of diiron-containing interfacial membrane proteins using the univector recombination system, *Protein Sci. 12*, 124−134.
37. Zhao, Q., Frederick, R., Seder, K., Thao, S., Sreenath, H., Peterson, F., Volkman, B. F., Markley, J. L., and Fox, B. G. (2004) Production in two-liter beverage bottles of proteins for NMR structure determination labeled with either ^{15}N- or ^{13}C-^{15}N, *J. Struct. Funct. Genomics 5*, 87−93.
38. Zwahlen, C., Legault, P., Vincent, S. J. F., Greenblatt, J., Konrat, R., and Kay, L. E. (1997) Methods for Measurement of Intermolecular NOEs by Multinuclear NMR Spectroscopy: Application to a Bacteriophage λ N-Peptide/*boxB* RNA Complex, *J. Am. Chem. Soc. 119*, 6711−6721.
39. Farrow, N. A., Muhandiram, R., Singer, A. U., Pascal, S. M., Kay, C. M., Gish, G., Shoelson, S. E., Pawson, T., Forman-Kay, J. D., and Kay, L. E. (1994) Backbone dynamics of a free and phosphopeptide-complexed Src homology 2 domain studied by ^{15}N NMR relaxation, *Biochemistry 33*, 5984−6003.
40. Altieri, A. S., Hinton, D. P., and Byrd, R. A. (1995) Association of biomolecular systems via PFG-NMR diffusion measurements, *J. Am. Chem. Soc. 117*, 7566−7567.
41. Ilyina, E. E., Roongta, V., Pan, H., Woodward, C., and Mayo, K. H. (1997) A pulsed-field gradient NMR study of bovine pancreatic trypsin inhibitor self-association, *Biochemistry 36*, 3383−3388.
42. Delaglio, F., Grzesiek, S., Vuister, G. W., Zhu, G., Pfeifer, J., and Bax, A. (1995) NMRPipe: a multidimensional spectral processing system based on UNIX pipes, *J. Biomol. NMR 6*, 277−293.
43. Cornilescu, G., Delaglio, F., and Bax, A. (1999) Protein backbone angle restraints from searching a database for chemical shift and sequence homology, *J. Biomol. NMR 13*, 289−302.
44. Herrmann, T., Güntert, P., and Wüthrich, K. (2002) Protein NMR structure determination with automated NOE assignment using the new software CANDID and the torsion angle dynamics algorithm DYANA, *J. Mol. Biol. 319*, 209−227.
45. Buchko, G. W., Rozek, A., Hoyt, D. W., Cushley, R. J., and Kennedy, M. A. (1998) The use of sodium dodecyl sulfate to model the apolipoprotein environment. Evidence for peptide-SDS complexes using pulsed-field-gradient NMR spectroscopy, *Biochim. Biophys. Acta 1392*, 101−108.
46. Rozek, A., Sparrow, J. T., Weisgraber, K. H., and Cushley, R. J. (1999) Conformation of human apolipoprotein C-I in a lipid-mimetic environment determined by CD and NMR spectroscopy, *Biochemistry 38*, 14475−14484.
47. Wang, G., Sparrow, J. T., and Cushley, R. J. (1997) The helix-hinge-helix structural motif in human apolipoprotein A-I determined by NMR spectroscopy, *Biochemistry 36*, 13657−13666.
48. Eliezer, D., Kutluay, E., Bussell, R., Jr., and Browne, G. (2001) Conformational properties of alpha-synuclein in its free and lipid-associated states, *J. Mol. Biol. 307*, 1061−1073.
49. le Maire, M., Champeil, P., and Moller, J. V. (2000) Interaction of membrane proteins and lipids with solubilizing detergents, *Biochim. Biophys. Acta 1508*, 86−111.
50. This reference was deleted on revision.
51. Papavoine, C. H., Konings, R. N., Hilbers, C. W., and van de Ven, F. J. (1994) Location of M13 coat protein in sodium dodecyl sulfate micelles as determined by NMR, *Biochemistry 33*, 12990−12997.
52. Bisaglia, M., Tessari, I., Pinato, L., Bellanda, M., Giraudo, S., Fasano, M., Bergantino, E., Bubacco, L., and Mammi, S. (2005) A topological model of the interaction between alpha-synuclein and sodium dodecyl sulfate micelles, *Biochemistry 44*, 329−339.
53. Chupin, V., Leenhouts, J. M., de Kroon, A. I., and de Kruijff, B. (1996) Secondary structure and topology of a mitochondrial presequence peptide associated with negatively charged micelles. A 2D H-NMR study, *Biochemistry 35*, 3141−3146.
54. Piserchio, A., Bisello, A., Rosenblatt, M., Chorev, M., and Mierke, D. F. (2000) Characterization of parathyroid hormone/receptor interactions: structure of the first extracellular loop, *Biochemistry 39*, 8153−8160.
55. Monticelli, L., Pedini, D., Schievano, E., Mammi, S., and Peggion, E. (2002) Interaction of bombolitin II with a membrane-mimetic environment: an NMR and molecular dynamics simulation approach, *Biophys. Chem. 101−102*, 577−591.
56. Rozek, A., Friedrich, C. L., and Hancock, R. E. (2000) Structure of the bovine antimicrobial peptide indolicidin bound to dodecylphosphocholine and sodium dodecyl sulfate micelles, *Biochemistry 39*, 15765−15774.
57. Papavoine, C. H., Remerowski, M. L., Horstink, L. M., Konings, R. N., Hilbers, C. W., and van de Ven, F. J. (1997) Backbone dynamics of the major coat protein of bacteriophage M13 in detergent micelles by ^{15}N nuclear magnetic resonance relaxation measurements using the model-free approach and reduced spectral density mapping, *Biochemistry 36*, 4015−4026.
58. Ma, D., Liu, Z., Li, L., Tang, P., and Xu, Y. (2005) Structure and dynamics of the second and third transmembrane domains of human glycine receptor, *Biochemistry 44*, 8790−8800.
59. Dyson, H. J., and Wright, P. E. (2005) Intrinsically unstructured proteins and their functions, *Nat. Rev. Mol. Cell Biol. 6*, 197−208.
60. Wright, P. E., and Dyson, H. J. (1999) Intrinsically unstructured proteins: re-assessing the protein structure-function paradigm, *J. Mol. Biol. 293*, 321−331.
61. Dunker, A. K., Cortese, M. S., Romero, P., Iakoucheva, L. M., and Uversky, V. N. (2005) Flexible nets. The roles of intrinsic disorder in protein interaction networks, *FEBS J. 272*, 5129−5148.
62. Csizmok, V., Bokor, M., Banki, P., Klement, E., Medzihradszky, K. F., Friedrich, P., Tompa, K., and Tompa, P. (2005) Primary contact sites in intrinsically unstructured proteins: the case of calpastatin and microtubule-associated protein 2, *Biochemistry 44*, 3955−3964.
63. Dyson, H. J., and Wright, P. E. (2002) Coupling of folding and binding for unstructured proteins, *Curr. Opin. Struct. Biol. 12*, 54−60.
64. Demchenko, A. P. (2001) Recognition between flexible protein molecules: induced and assisted folding, *J. Mol. Recognit. 14*, 42−61.
65. Aivazian, D., and Stern, L. J. (2000) Phosphorylation of T cell receptor zeta is regulated by a lipid dependent folding transition, *Nat. Struct. Biol. 7*, 1023−1026.
66. Pfander, R., Neumann, L., Zweckstetter, M., Seger, C., Holak, T. A., and Tampe, R. (1999) Structure of the active domain of the herpes simplex virus protein ICP47 in water/sodium dodecyl sulfate solution determined by nuclear magnetic resonance spectroscopy, *Biochemistry 38*, 13692−13698.

67. Chandra, S., Chen, X., Rizo, J., Jahn, R., and Sudhof, T. C. (2003) A broken alpha -helix in folded alpha-Synuclein, *J. Biol. Chem. 278*, 15313−15318.
68. Nield, J., Kruse, O., Ruprecht, J., da Fonseca, P., Buchel, C., and Barber, J. (2000) Three-dimensional structure of *Chlamydomonas reinhardtii* and *Synechococcus elongatus* photosystem II complexes allows for comparison of their oxygen-evolving complex organization, *J. Biol. Chem. 275*, 27940−27946.
69. Nield, J., Orlova, E. V., Morris, E. P., Gowen, B., van Heel, M., and Barber, J. (2000) 3D map of the plant photosystem II supercomplex obtained by cryoelectron microscopy and single particle analysis, *Nat. Struct. Biol. 7*, 44−47.
70. Yakushevska, A. E., Keegstra, W., Boekema, E. J., Dekker, J. P., Andersson, J., Jansson, S., Ruban, A. V., and Horton, P. (2003) The structure of photosystem II in *Arabidopsis*: localization of the CP26 and CP29 antenna complexes, *Biochemistry 42*, 608−613.
71. Nield, J., Redding, K., and Hippler, M. (2004) Remodeling of light-harvesting protein complexes in *Chlamydomonas* in response to environmental changes, *Eukaryotic Cell 3*, 1370−1380.
72. Kargul, J., Turkina, M. V., Nield, J., Benson, S., Vener, A. V., and Barber, J. (2005) Light-harvesting complex II protein CP29 binds to photosystem I of *Chlamydomonas reinhardtii* under State 2 conditions *FEBS J. 272*, 4797−4806.
73. Takahashi, H., Iwai, M., Takahashi, Y., and Minagawa, J. (2006) Identification of the mobile light-harvesting complex II polypeptides for state transitions in *Chlamydomonas reinhardtii*, *Proc. Natl. Acad. Sci U.S.A. 103*, 477−482.
74. Turkina, M. V., Kargul, J., Blanco-Rivero, A., Villarejo, A., Barber, J., and Vener, A. V. (2006) Environmentally modulated phosphoproteome of photosynthetic membranes in the green alga *Chlamydomonas reinhardtii*, *Mol. Cell Proteomics 5*, 1412−1425.
75. Koradi, R., Billeter, M., and Wüthrich, K. (1996) MOLMOL: a program for display and analysis of macromolecular structures, *J. Mol. Graphics 14*, 51−55.
76. Kyte, J., and Doolittle, R. F. (1982) A simple method for displaying the hydropathic character of a protein, *J. Mol. Biol. 157*, 105−132.

BI062148M